Stopping power in nonideal and strongly coupled plasmas

K. Morawetz and G. Röpke
Max-Planck-Gesellschaft, AG ''Theoretische Vielteilchenphysik'' an der Universität Rostock, 18055 Rostock, Germany
(Received 18 March 1996)

The stopping power of dense nonideal plasmas is calculated in different approximations. The T-matrix approximation for binary collisions is compared with the random phase approximation for dielectric fluctuations. Within a microscopic model, the dynamical evolution of the velocity of the projectile is calculated. It reproduces well experimental values for the stopping of fast heavy ions. A comparison with molecular dynamical simulation is performed for the friction coefficient. It is found that the T matrix reproduces the simulation result with a charge dependence of $\xi^{1.4}$, where $\xi = Z\Gamma^{3/2}$. The connection to transport properties like conductivity is presented. In this way we extend former small Γ expansions to strongly coupled plasmas. Further improvements due to correlations are discussed. Both concepts, cluster decomposition and memory, are compared and it is found that they lead to the same quantum virial corrections of Beth-Uhlenbeck type in equilibrium. However, memory in the kinetic equation causes an additional renormalization of the effective energy transfer in nonequilibrium. [S1063-651X(96)08409-7]

PACS number(s): 52.20.−j, 52.40.Mj, 05.20.Dd, 82.20.Mj

I. INTRODUCTION

Stopping power is an often investigated quantity. One must know how much energy can be deposited in a small volume, which has direct relevance for the prospect of inertial fusion [1]. Experiments have shown that the stopping power can be enhanced an order of magnitude due to stopping of heavy ions in a nonideal plasma in comparison with a cold gas as target [2]. Therefore it is important to study the underlying microscopic processes.

While most treatments solve the coupled Vlasov equation with the self-consistent Poisson equation [3] only a few attempts are made to incorporate higher order correlations. This is basically due to the fact that at very large projectile velocities the mean field approximation leads to quite good results using Bethe-type formulas of the stopping power [4]. In the strong coupling limit the numerical solution of the coupled Poisson-Vlasov equation leads to large differences from the linear theory [5]. However, with respect to the fact that the coupled Poisson and Vlasov equations are mean field equations, it is certainly necessary to consider higher order diagrams if one would like to describe strongly coupled plasmas. This is also due to the reversible character of the Vlasov equation, such that one has to incorporate collisions to provide energy spreading and stopping. Recently comparisons with molecular dynamical simulations [6] clearly show the importance of collisions. This calculation as well as experimental measurements [7] show a deviation from the charge dependence of the stopping power at small velocities predicted by the linear theory.

A further question that arises is the dynamical evolution of the effective projectile charge. In [3] a master equation was solved including different processes contributing to the one step ionization. Recent measurements point to the importance of multi-ionization processes. An extension of the theory of stopping power was given by the inclusion of a structure factor for the projectile ion as a multicharged cluster [8–11]. Therein, the correlated stopping of clusters is considered and the relevance of structure effects in dense plasmas is shown. Later it was found that the enhancement of the stopping power due to ion-ion correlations in weakly coupled plasmas is suppressed in the strong coupling regime [6]. These constructive interference effects are disturbed by the collisions between target electrons. A promising treatment of strongly coupled plasmas employs wave packet molecular dynamics [12]. There the electrons are represented by Gaussian wave packets, whose parameters follow a pseudo-Hamiltonian dynamics.

Here we follow a kinetic approach within the quantum statistical framework. We present the results obtained within different approximations resulting in different quantum collision integrals. These calculations continue earlier investigations [13–15] where random phase approximation (RPA) and T-matrix approximation have been considered. The outline of the paper is as follows. In the second section we give an alternative derivation of the RPA stopping power, which shows that the known formula is also valid for degenerate plasmas. Then different limiting cases are compared with the exact numerical solution. In Sec. III we derive the binary collision component of the stopping power. Both expressions, T matrix and RPA, are combined and the numerical results are presented for quantum mechanical T-matrix and RPA calculations. It is found that the RPA by itself is higher for dense, strongly coupled plasmas, where the collective transport of energy is dominant. In Sec. IV we present the dynamical solution for the velocity of projectiles and compare with experimental values. There we describe the penetration of a fast heavy ion in a dense, nonideal plasma by assuming that the surrounding plasma is in equilibrium. The experimental results are reproduced well. The comparison with molecular dynamical simulations is performed in Sec. V. We find that the T-matrix approximation can describe the friction coefficient, which is the stopping power at small velocities, for strongly coupled plasmas. In Sec. VI we give a short discussion of possible extensions of the theory in order to incorporate correlations. The correlations are introduced via two different concepts; both the cluster decomposition in the polarization function and the memory effects lead to

quantum virial corrections of Beth-Uhlenbeck type in equilibrium. However, the memory effects are an expression of nonideality [16] and lead to an additional renormalization of the stopping power. We will demonstrate that this renormalization can account for further deviations from the charge dependence of linear theory scaling.

II. STOPPING POWER BY DIELECTRIC FLUCTUATIONS

The long range fluctuations due to density oscillations are described by the random phase approximation. Within this approximation (see Fig. 1) the corresponding kinetic equation is the Lennard-Balescu kinetic equation whose collision integral can be derived including external electric fields (laser fields) and memory effects [17]. The field influences the collision integral is two main ways. First, it widens the δ distribution of energy conservation by an oscillating part $\sim E^2$, and secondly, some retardation occurs which causes a non-Markovian behavior of the collision integral.

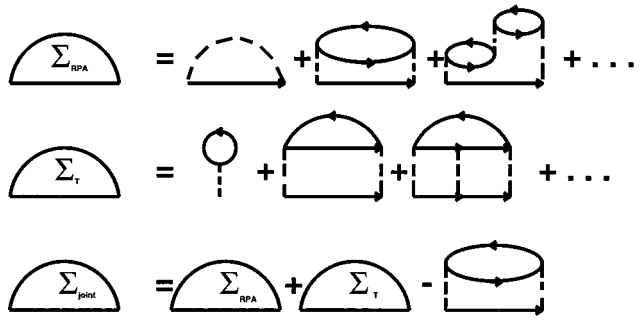

FIG. 1. The RPA approximation for the self-energy (above) as well as T-matrix approximation (middle). The joint expression counts the Fock term twice and has to be subtracted (below).

A. Stopping power in RPA

In the following we first neglect the memory effects, which will be treated later in Sec. VI. Then the Lennard-Balescu collision integral reads

$$I_a^{\mathrm{LB}}(p;R,t)=\frac{2\pi}{\hbar}\sum_b \int \frac{dp_a' dp_b dp_b'}{(2\pi\hbar)^6}\delta(p_a+p_b-p_a'-p_b')\,\delta(E_p^a+E_p^b-E_p^{a'}-E_p^{b'})[f_{a'}f_{b'}\overline{f_a}\,\overline{f_b}-f_a f_b\overline{f_{a'}}\,\overline{f_{b'}}]$$
$$\times|\mathcal{V}_{ba}(p_a'-p_a,E_p^{a'}-E_p^a;R,t)|^2, \tag{1}$$

with the one-particle distribution function $f_a=f(p_a;R,t)$ of species a and correspondingly $\overline{f_a}=(1-f_a)$ and the quasiparticle energy $E_p^a=E^a(p;R,t)$. Here a mixed representation is used where p is the transform of difference coordinates, R the center of mass coordinate, and t the center of mass time. The kinetic equation (1) is a complicated coupled equation including the screened potential $\mathcal{V}$ which is connected to the response function ε by

$$\mathcal{V}_{ab}(q,\omega,R,t)=V_{ab}(q)\varepsilon^{-1}(q,\omega,R,t), \tag{2}$$

where V_{ab} is the Coulomb potential and the dielectric function ε is given in quasiparticle approximation as

$$\varepsilon(p,\omega;R,t)=1+\sum_b V_{bb}(p)\Pi_b^0(p,\omega;R,t)=1+\sum_b V_{bb}(p)\int\frac{d\overline{p}}{(2\pi\hbar)^3}\frac{[f_b(\overline{p}-p;R,t)-f_b(\overline{p};R,t)]}{\omega-E^b_{\overline{p}-p}+E^b_{\overline{p}}+i\eta}. \tag{3}$$

Here Π^0 denotes the polarization function of the single-particle loop. Restricting to the free particle dispersion we can write the energy transfer rate per time from Eq. (1) in the form

$$\dot{E}_a=\left\langle\frac{p^2}{2m_a}\dot{f}_a\right\rangle$$
$$=\frac{2\pi}{\hbar}\sum_b\int\frac{d^3p\,d^3q\,d^3Q}{(2\pi\hbar)^9}\delta(E_p^a+E_Q^b-E_{p+q}^a-E_{Q-q}^b)$$
$$\times\frac{E_p^a-E_{p+q}^a}{2}|\mathcal{V}_{ab}(q,E_p^a-E_{p+q}^a)|^2[f_{p+q}^a f_{Q-q}^b(1-f_Q^b)$$
$$-f_p^a f_Q^b(1-f_{Q-q}^b)-f_p^a f_{p+q}^a(f_{Q-q}^b-f_Q^b)]. \tag{4}$$

The momentum conservation has been integrated out and the statistical occupation factors have been rearranged. In view of the aim of describing fast particles stopped in a surrounding plasma, we assume that the projectile possesses a very sharp distribution around its velocity. This velocity $v(t)$ is time dependent, while the target plasma is assumed to be in equilibrium with the one-particle Fermi distribution function $f_b(E)$. For the projectile we have $f_a(p)=(2\pi\hbar)^3 n_a\delta(p-u(t))$ where $u(t)=m_a v(t)$ and n_a is the artificial density of the beam. Then the last term of the occupation factors in (4) vanishes and we derive

$$\dot{E}_a=\frac{2\pi}{\hbar}n_a\sum_b\int\frac{d^3q\,d^3Q}{(2\pi\hbar)^6}\delta(\hbar\omega+E_Q^b-E_{Q-q}^b)\hbar\omega n_B(\hbar\omega)$$
$$\times\mathcal{V}_{ab}(\omega,q)^2(f_{Q-q}^b-f_Q^b)\frac{d\omega}{2\pi}, \tag{5}$$

where the abbreviation $\hbar\omega=E_{u-q}^a-E_u^a$ and the Bose occupation function n_B have been introduced. We can now pro-

ceed with $\mathcal{V}_{ab}^2 = V_{aa}V_{bb}/|\varepsilon|^2$, which follows from the RPA in Eq. (2), and introduce the dielectric function (3) to obtain the final result

$$\dot{E}_a = -\frac{2n_a}{\hbar}\int \frac{d^3q}{(2\pi\hbar)^3}\hbar\omega n_B(\hbar\omega)V_{aa}(q)^2 \mathrm{Im}\varepsilon^{-1}(q,\hbar\omega). \tag{6}$$

As one sees, the sum over different species is subsumed into the dielectric function. It is noteworthy to remark that this result is valid for any arbitrary degeneracy. The presented derivation shows that the result (6) is more generally valid than those derived earlier [13–15]. Especially, the free energy dispersion is replaced by the quasiparticle one. Here we derived (6) only within RPA. However, higher order correlations like vertex corrections can be incorporated in the dielectric function, such that (6) remains valid, which will be discussed in Sec. VI. This fact is important for dense solid state plasmas which have been used recently for stopping experiments. There the result (6) is applicable as well.

A more explicit form can be given by carrying out the angular integration

$$\frac{\dot{E}_a}{n_a} = \frac{2e_a^2}{\pi\varepsilon_0}\frac{1}{v(t)}\int_0^\infty \frac{dk}{k}\int_{-v(t)k+\hbar k^2/2m_a}^{v(t)k+\hbar k^2/2m_a} d\omega\omega n_B(\omega) \times \mathrm{Im}\varepsilon^{-1}(\hbar k,\omega). \tag{7}$$

If we had used the momentum transfer $F=\dot{p}_a/n_a$ for the stopping power instead of the energy transfer rate we would have to replace the ω factor in (7) by the term $(\omega-\hbar k^2/2m_a)/v(t)$. Because we restrict ourselves to heavy ions this difference is not important here.

B. High velocity limit

In the case of velocities much larger than the thermal velocity and/or very heavy ions with mass m_a, the integration limits in (7) can be extended to $\pm\infty$. Then the sum rule (B1) leads to the result

$$\frac{\dot{E}_a}{n_a} = \frac{e_a^2\omega_p^2}{\varepsilon_0 v(t)}\int \frac{dk}{k}, \tag{8}$$

with the plasma frequency ω_p. The expression shows the typical logarithmic divergence for small and large wavelength k. Let us remark that this divergence is absent in the complete expression (7) for small wave vectors due to screening and for large wave vectors due to quantum effects which are mainly reflected in the de Broglie wavelength. The loss of both, screening as well as quantum effects, during the approximation which leads from (7) to (8), is often reintroduced by cutoff procedures. For large wave vectors, one assumes a maximal $k_{\max}$ and the small wave vectors are limited mainly by the collective mode ω_p/v, see [18]. The well known Bethe-type formula is obtained by using the de Broglie wavelength as maximal wave vector

$$\frac{\dot{E}_a}{n_a} = \frac{Z_a^2e^2\omega_p^2}{\varepsilon_0 v(t)}L_{\mathrm{Bethe}}, \tag{9}$$

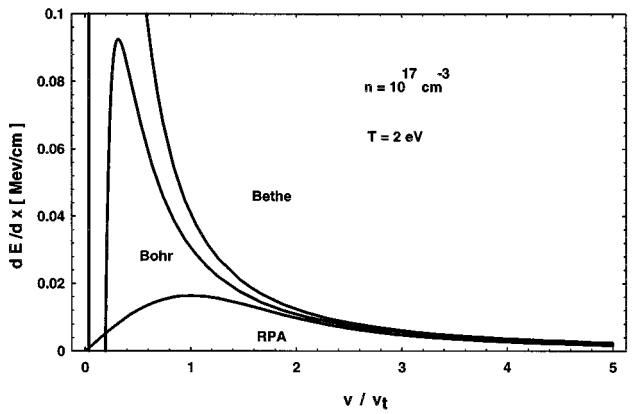

FIG. 2. The RPA stopping power for a $^{238}U^{1+}$ projectile in comparison with the classical Bohr (10) and the quantum Bethe (9) result.

with the Coulomb logarithm $L_{\mathrm{Bethe}}=\ln(2v^2m/\omega_p\hbar)$. For parameters resembling classical transport the maximal wave vector is often calculated by the shortest colliding distance $k_{\max}=mv^2\varepsilon_0/Z_ae^2$ of two particles which leads to the classical Bohr result

$$\frac{\dot{E}_a}{n_a} = \frac{Z_a^2e^2\omega_p^2}{\varepsilon_0 v(t)}L_{\mathrm{Bohr}}, \tag{10}$$

with $L_{\mathrm{Bohr}}=\ln(v^3m\varepsilon_0/\omega_pZ_ae^2)$. Note that within the approximation (10) one uses a concept (colliding two particle, nearest distance) which is not included *a priori* in the original collision integral (1). Instead, if we wish to consider the collision dominated regime we have to use the T-matrix approximation in the next section. This will lead to the same limiting formula. But it is already presented here in order to illustrate the close relation between different approximation schemes. Various limiting cases and improvements of approximative formulas have been discussed in the literature, see [14], and citations therein.

All approximative as well as exact formulas show that the stopping power is essentially proportional to the squared plasma frequency of the target plasma. Therefore the contribution of ions with much larger mass can often be neglected in comparison to the electron contribution of the target plasma.

C. Numerical results

Here we would like to discuss the validity of the approximation formulas (9) and (10) in comparison with the exact result (7). In Fig. 2 the stopping power $dE/dx=\dot{E}/n_av$ of a projectile with mass number 238 and charge $Z=1$ in a plasma with density $10^{17}\mathrm{cm}^{-3}$ and a temperature of 2 eV is plotted versus velocity. One sees that the approximative formulas are in agreement with the exact numerical result for velocities higher than two times the thermal velocity. The disagreement for smaller velocities is quite obvious.

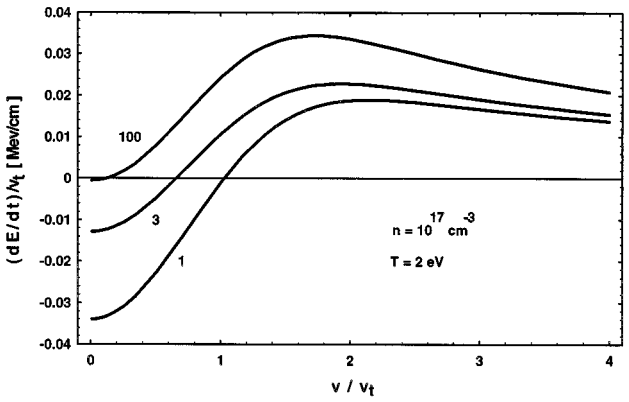

FIG. 3. The RPA stopping power $\dot{E}$ for mass ratios between projectiles and target of 1,3,100 versus velocity.

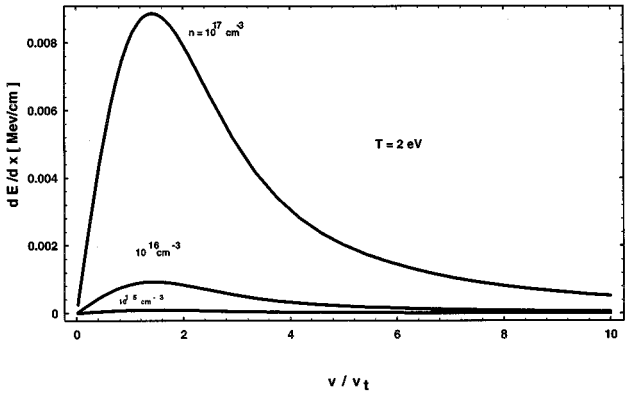

FIG. 4. The stopping power for $^{238}U^{1+}$ versus velocity for different densities at a temperature of 2eV.

The careful inspection of the numerical result of the exact RPA stopping power formula (7) leads to a zero at small velocities. In Fig. 3 the stopping power for three different mass ratios is plotted versus velocity. This zero scales with the mass ratio between target and projectile [15]. It shows that for projectile velocities smaller than the thermal velocity of the target plasma (scaled by mass ratio), the projectile will be accelerated up to the temperature of the surrounding plasma. This describes the fact that subsonic projectiles can absorb plasmons but not emit them [15] (also known as the acoustic Cherenkov effect).

Next we discuss the temperature as well as density dependence of the exact RPA stopping power. In Fig. 4 the stopping power for $^{238}U^{1+}$ is plotted versus velocity for different densities. With increasing density of the target plasma the stopping power is increased. This is further expressed in Fig. 5 where the stopping power is plotted at thermal velocity versus density for different temperatures. One sees that for lower temperature the increase with density is more rapid than for higher temperatures. A cold plasma can absorb many more phonons than a hot plasma can. At higher temperature a plasma becomes ideal, which means that the interaction and therefore the RPA stopping is much lower than the thermal motion and we expect that binary collisions are dominating.

III. STOPPING POWER BY COLLISIONS

We now proceed and calculate the contribution of strong collisions to the stopping power. Therefore we restrict ourselves to binary collision approximation and give the self-energy in terms of the ladder summation (see Fig. 1). Then the corresponding collision integral reads

$$I_a^{\mathrm{Boltz}}(p,T)=\frac{2\pi}{\hbar}\sum_b \int \frac{d^3p_a' d^3p_b d^3p_b'}{(2\pi\hbar)^6}\delta(p_a+p_b-p_a'-p_b')\,\delta(E^a(p)+E^b(p)-E^{a'}(p)-E^{b'}(p))$$
$$\times[f_{a'}f_{b'}\overline{f_a}\overline{f_b}-f_a f_b\overline{f_{a'}}\overline{f_{b'}}]|\langle p_a p_b|\mathcal{T}_{ba}^R(E_p^{a'}-E_p^a)|p_a' p_b'\rangle|^2, \tag{11}$$

where the ladder summation is represented by the T matrix. The latter one can be expressed by the quantum mechanical differential cross section. After a straightforward algebra (Appendix A) we obtain for the energy transfer rate, in a manner analogous to that of the preceding section for a nondegenerate plasma,

$$\frac{\dot{E}}{n_a}(v)=\sum_b \frac{n_b v_t}{m_b^2\sqrt{\pi}}\frac{e^{-m_b v^2/2T}}{v}\int_0^\infty dp\,p^2\sigma_{ab}^t(p)\left[a\cosh a-\left(1+\frac{p^2(1+m_b/m_a)}{m_a T}\right)\sinh a\right]e^{-(p^2/2m_bT)(1+m_b/m_a)^2}, \tag{12}$$

with the thermal velocity $v_t^2=2T/m_b$ and the abbreviation $a=(vp/T)(1+m_b/m_a)$. The quantum mechanical transport cross section was introduced as

$$\sigma^t(p)=\int d\Omega(1-\cos\theta)\frac{d\sigma}{d\Omega}. \tag{13}$$

A. Quantum transport cross sections

This cross section is obtained by solving the Schrödinger equation and using the representation of the T matrix in terms of scattering phase shifts. In [19] a fit formula is given which subsumed the numerical results for the transport cross section for a plasma with charge $Z=1$,

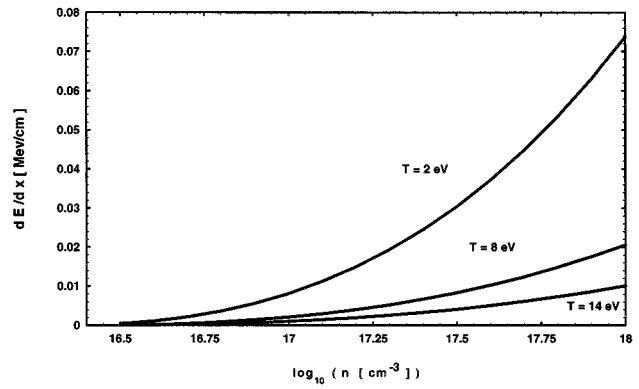

FIG. 5. The stopping power for $^{238}U^{1+}$ at thermal velocity, which is nearly the maximum of the stopping power, versus densities for different temperatures.

$$\frac{k^4 a_B^2}{4\pi}\sigma^t(k)=a_0\ln\left\{\epsilon^2\frac{1+a_4\eta}{a_1+a_2\eta+a_3\eta^2}\times\left[1+a_5\ln\left(\frac{a_6}{\epsilon}+1\right)\right]^2+1\right\}, \tag{14}$$

with $\eta=\pi^{-2}k^2a_B^2$ and $\epsilon=k^2a_B r_{\rm Deb}/2$. The parameter a_0-a_6 as well as the effective Debye radius $r_{\rm Deb}$ can be found in [19]. This formula interpolates the data for the transport cross section using a static screened Debye potential with effective Debye radius. The coefficients a_2,a_3,a_4 are chosen to reproduce the Born approximation for $\eta\gg1$ and the first and second WKB approximation for small quantum corrections $\eta\ll1$. The parameters a_5 and a_6 are introduced to fit the behavior of the cross section in the quasiclassical limit for small values of ϵ.

B. Classical limit

Expression (12) can be simplified if we use for the transport cross section the classical approximation which reads [6]

$$\sigma^t(p)=2\pi b_0^2\ln\left(1+\frac{b_m^2}{b_0^2}\right), \tag{15}$$

with $b_0=e^2\mu Z_a/p^2$, μ the reduced mass, and the maximum impact parameter b_m. Further, we consider large projectile velocities and heavy ions where we can replace the momentum dependence of the logarithm by the mean value $\langle p\rangle\approx\mu\sqrt{\langle v^2+v_t^2\rangle}$. Then the cross section in (12) can be taken out of the integral and the stopping power becomes

$$\frac{\dot E_a}{n_a}=\frac{\omega_p^2e_a^2}{\varepsilon_0}\frac{L_C}{v}\left[\mathrm{erf}\left(\frac{v}{v_t}\right)-2\frac{v}{v_t\sqrt{\pi}}e^{-(v/v_t)^2}\right], \tag{16}$$

with the Coulomb logarithm

$$L_C=\sum_b\frac{1}{2}\ln\left(1+\frac{(v_t^2+2v^2)(v^2+v_t^2)^2m_b^2\varepsilon_0^2}{2\omega_p^2e_a^2e_b^2}\right). \tag{17}$$

Here we have used a mean value for the maximal impact parameter $b_m=(1/\kappa)\sqrt{1+2(v/v_t)^2}$ such that it takes the value κ^{-1} for small velocities and v/ω_p for fast projectiles where the collective mode limits the reaction time. The limiting expression within the Coulomb logarithm approximation (16) coincides with the derivation in [6,20] which has been derived by an entirely different way.

As one sees, expression (17) approaches the limit

$$L_c=\ln\frac{v^3m_b\varepsilon_0}{\omega_pe_ae_b} \tag{18}$$

for large projectile velocities. Therefore Eq. (16) yields the classical result (10).

C. Born approximation

Instead of the classical cutoff used in the preceding section, we now employ the quantum Born approximation of the T matrix. Thus we use a screened potential which corresponds to the cutoff for small momenta by the inverse Debye screening length κ and at large momenta by the thermal de Broglie wavelength due to quantum effects. The transport cross section then reads

$$\sigma^t(p)=\frac{2\pi\hbar^4}{p^4a_B^4}\left[\ln(1+4b)-\frac{4b}{1+4b}\right], \tag{19}$$

with a_B the Bohr radius and $b=p^2/\hbar^2\kappa^2$. Following now the same approximations used in the preceding section, which means we use $p\approx\mu\sqrt{v^2+v_t^2}$, we arrive instead of (17) at

$$L_C=\sum_b\frac{1}{2}\left(\ln(1+4c_b)-\frac{4c_b}{1+4c_b}\right), \tag{20}$$

with

$$c_b=\frac{(v_t^2+2v^2)(v^2+v_t^2)m_b^2}{2\omega_p^2\hbar^2}.$$

For large projectile velocities it approaches the limit

$$L_C=\ln\left(\frac{2mv^2}{e\hbar\omega_p}\right), \tag{21}$$

which leads just to the known Bethe result (9), but with an e^{-1} factor in the logarithm. This represents (7) in the limit of large velocities better than (9). Therefore the quantum-Born approximation leads to an enhanced Bethe result for large projectile velocities. We also point out the different charge dependencies in (17) and (20) due to the different cutoffs.

D. Joint expressions

To consider both the stopping power due to dielectric fluctuations and due to binary collisions one would add Eqs. (12) and (7). The inspection of the corresponding diagrams in Fig. 1 shows that the Fock term is double counted by this way. Hence the Born term of (7) or (12) has to be subtracted. This expression, called here the joint expression, is well known [21,22].

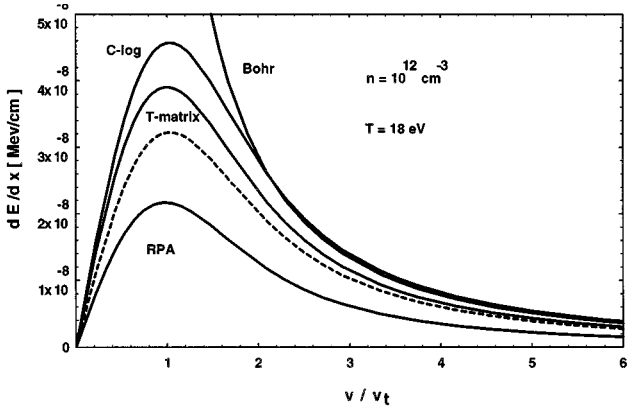

FIG. 6. The stopping power calculated by RPA in (7), T matrix in (12), and the Coulomb logarithm approximation (16) together with the classical Bohr result (dashed) in (10) versus velocity for low density and high temperature. A projectile with charge $Z=1$ and a mass of ^{238}U was chosen. The dotted line represents the joint expression result ($I_{\mathrm{LB}}+I_{\mathrm{Boltz}}-I_{\mathrm{Landau}}$).

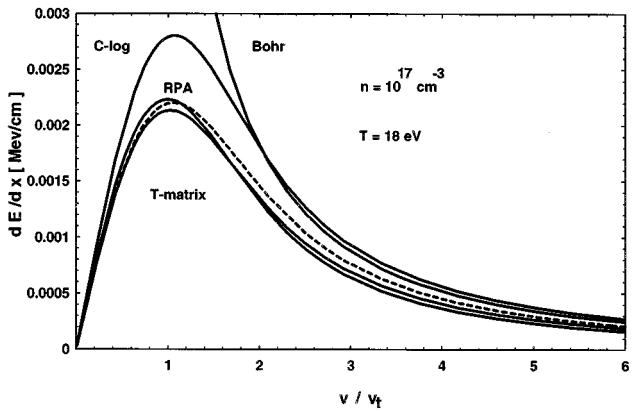

FIG. 7. The stopping power as in Fig. 6 calculated by RPA, T matrix, and Coulomb logarithm together with the classical Bohr result versus velocity for high density and high temperature.

Evaluating the Born term leads to expression (7) but with $-\mathrm{Im}\varepsilon$ instead of $\mathrm{Im}\varepsilon^{-1}$. It is interesting to consider the limit of large velocities in the same manner as it was done in Sec. II B. Using the sum rule (B2) for the corresponding expression with $-\mathrm{Im}\varepsilon$ instead of $\mathrm{Im}\varepsilon^{-1}$ we get just the RPA result (8). Because this has to be subtracted, the joint expression consists therefore only of the binary collision term (16) or (10) in the limit of large velocities. This shows clearly that in the large velocity domain the stopping power is dominated by the binary collisions. This fact was observed also in [23] where the enhancement of the stopping power due to dielectric theory in a strongly correlated plasma is destroyed by collisions, which was found in agreement with molecular dynamical simulations. Therefore the collisions dominate in the strong coupling regime due to the charge dependence. It has to be remarked that the Born term with bare Coulomb potential is divergent in contrast to the RPA result as it is known from the Landau collision integral. Therefore the numerical evaluation of the Born term in (7) is only meaningful with, e.g., a statically screened Coulomb potential.

The subtracting scheme does not mean that the RPA contribution can be neglected. Therefore we check in the following the case for $Z_a=1$. Instead of using approximative formulas for high velocities, Eq. (12) is calculated numerically with the help of the quantum mechanical transport cross sections. We see from the numerical solution of (7) and (12) that the RPA contribution becomes more important for dense plasmas at low temperatures. To illustrate this, Fig. 6 shows the stopping power of $^{238}\mathrm{U}^{1+}$ calculated from this different contribution. The density of $n=10^{12}$ cm^{-3} and temperature of $T=18$ eV are in the region where the plasma is ideal. One sees that the contribution due to binary collisions exceeds the contribution from RPA by a factor of 2. For higher velocities the expression approaches the classical Bohr result, which leads to unphysical high stopping power at projectile velocities around thermal velocity of the plasma. The approximation by the Coulomb logarithm (16) shows a rough agreement with the exact T-matrix result. The joint expression interpolates between the RPA result and the T matrix. In Fig. 7 we have chosen a higher density of $n=10^{17}$cm^{-3}. Here the RPA contribution is almost equal to the contribution from the binary collisions. The Coulomb logarithm approximation exceeds the T matrix remarkably. If we decrease the temperature of the plasma in Fig. 8, then the RPA contribution is larger than the binary collisions. This can be understood such that at low temperatures and high densities the collective behavior dominates the energy transfer, while at high temperatures and low densities the binary collisions dominate. The Coulomb logarithm coincides almost with the RPA result in Fig. 8 and overestimates the T matrix by about a factor of 2. We can conclude that stopping due to collective behavior, i.e., absorption and emission of plasmons, is the most important contribution in dense nonideal plasmas.

IV. COMPARISON WITH EXPERIMENTS OF HEAVY ION STOPPING

We describe the penetration of a projectile into the plasma by the following model assumptions. (i) The frequency of heavy ions should be lower than the inverse relaxation time of the plasma such that the plasma is in equilibrium. (ii) The beam of projectiles propagates in one dimension. (iii) The dynamical evolution of the projectile is described by its velocity

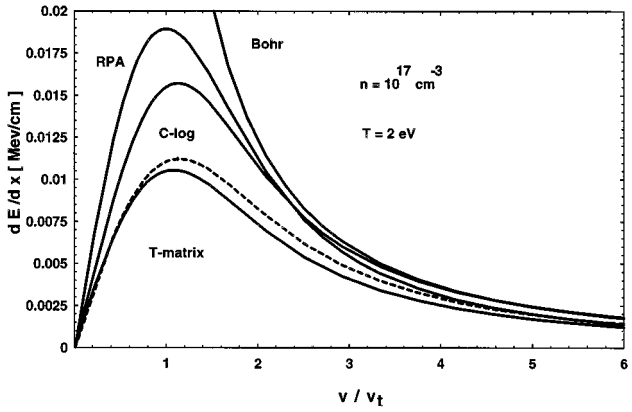

FIG. 8. The stopping power as in Fig. 6 calculated by RPA, T matrix, and Coulomb logarithm together with the classical Bohr result versus velocity for high density and low temperature.

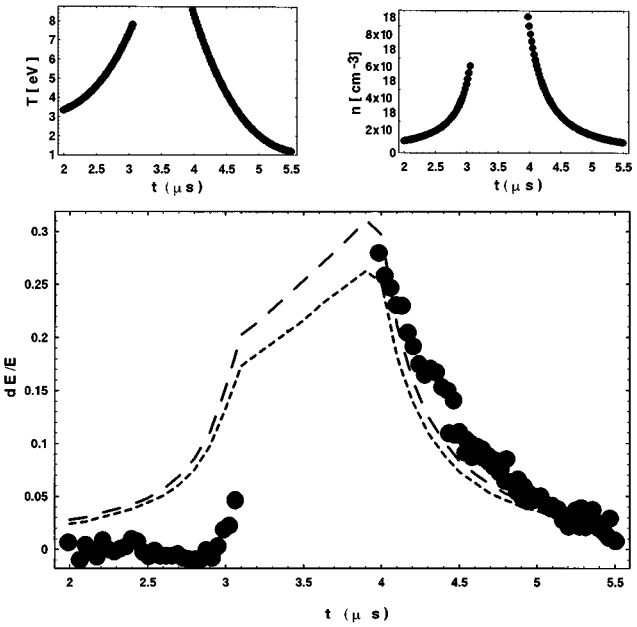

FIG. 9. The relative energy loss of $^{238}U^{53+}$ with $E_0=6.3$ MeV/u beam energy versus time of the Z pinch in an argon plasma. The experimental values (solid line) are from Wetzler *et al.* [24]. The theoretical curves (dashed) are calculated with the experimental density and temperature of the Z pinch as input. The lower dashed line corresponds to the classical result and the upper dashed line to the quantum result. The difference is mostly due to the different charge dependencies. The lack of data between 3 and 4 μs is due to the strong focusing force of the plasma current resulting in decreasing intensity of the beam after the plasma (plasma lens effect) [33,24]. The theoretical curves interpolate between 3 and 4 μs.

$$\dot{v}(t)=-\frac{F[v(t)]}{m_a},\quad v(0)=v_0, \tag{22}$$

where $F=[1/v(t)]\cdot(\dot{E}/n)$ represents the stopping power in terms of the energy transfer rate.

With the help of the derived stopping power we are now able to describe the dynamical evolution of the projectile. Thus we have to solve within this model the differential equation

$$\dot{v}(t)=-\frac{1}{v(t)}\frac{\dot{E}_a(v(t))}{m_a n_a}, \tag{23}$$

where the right hand side represents the stopping power in terms of the previously calculated energy transfer rate. For comparison with experiments we choose a data set for a beam of $^{238}U^{53+}$ with a beam energy of $E=6.3$ MeV/u on a hot argon plasma. This experiment was chosen because the mean charge state remains constant within this experiment, which was assumed during the entire calculation [24]. The experimental values of plasma density and temperature serve as an input for the stopping power calculation. The result can be seen in Fig. 9. The Z-pinch discharge occurs around the time point of 4 μs. We have plotted the comparison with the quantum result (20) and the classical result (17). Whereas the quantum results lead to a higher stopping power for high densities the classical result reproduces the experimental values more appropriately. This is understandable due to the different charge dependencies. In the classical result the cutoff is given due to the minimal distance, resulting in a charge dependence of the stopping power $Z_a^2\ln(1+c/Z_a^2)$. In contrast, the quantum cutoff is given due to the thermal de Broglie wavelength, which leads to a Z_a^2 dependence of the stopping power.

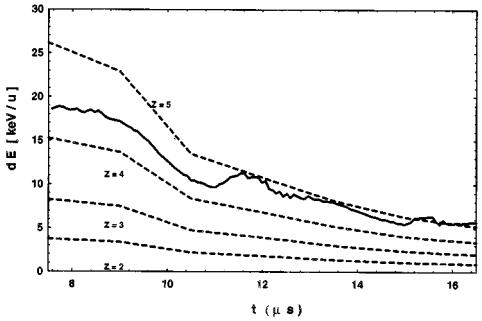

FIG. 10. The relative energy loss of ^{84}Kr with $E_0=45$ keV/u beam energy versus time of the Z pinch in a hydrogen plasma. The experimental values (solid line) are from [2]. The theoretical curves are calculated with different assumed charge states of the projectile for the experimental density and temperature of the Z pinch as input. One sees that the projectile charge reaches a charge state of 4/5.

The stopping after the pinch is described quite reasonably, but the energy loss before the pinch is overestimated. This can be explained because there is still a cold plasma while we calculate the stopping with formulas for hot nonideal plasmas.

Another experiment is chosen from [2]. Here the charge state of the projectile is changing during the penetration through the plasma. This is illustrated in Fig. 10 where we have calculated the stopping power for different charge states with the experimental density and temperature. One sees that the experimental stopping power can only be reproduced assuming that the charge is changing between $Z=4$ and $Z=5$. The charge dynamics can be treated within a phenomenological approach in [3]. From the microscopic point of view the dynamical evolution of the charge state has to be treated in a forthcoming work.

V. COMPARISON WITH MOLECULAR DYNAMICAL SIMULATIONS

The observation in the preceding section underlines the importance of the charge dependence of the stopping power, which plays an important role in current discussions. For instance, in [6] a comparison with molecular dynamical simulations yields a charge dependence of $Z_a^{1.4}$ at small velocities. Here we can discuss the stopping power (16) in comparison to the classical approximation (17) and the quantum result (20). Whereas the latter one shows only a Z_a^2 dependence, the classical result leads to a more involved dependence $Z_a^2\ln(1+c/Z_a^2)$. From the latter form we see that for special density and temperature dependent c any dependence between Z_a^2 and a constant can be approached with increasing charge. This is in clear disagreement with the results of the molecular dynamical simulations [6], where a $(Z_a\Gamma^{3/2})^{1.43}$ dependence was found pertaining to higher

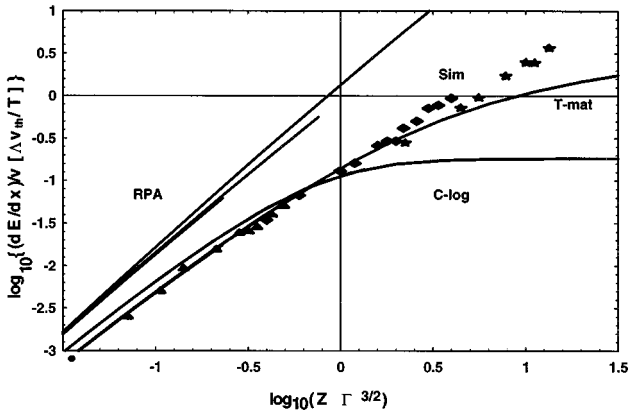

FIG. 11. A double logarithmic plot of the friction coefficient versus $Z\Gamma^{3/2}$ with the plasma parameter Γ. The points are the results from the simulation [6] for three different plasma parameters $\Gamma=0.11$ (crosses), $\Gamma=0.34$ (triangles), and $\Gamma=1.08$ (circles). The Coulomb approximation (16) is compared with the T-matrix approximation (12) and the RPA results (7) for three different temperatures $T=2,5,10$eV. While the Coulomb logarithm and the T matrix follow the scaling of the linear theory, the RPA result shows deviations with different temperatures.

charges and plasma parameter. This shows the limits of the weak coupling theory.

In Fig. 11 we plotted the result of the molecular dynamical simulation [6] with our different approximation schemes. The double logarithmic plot shows the friction coefficient which is just the stopping power at small velocities divided by the velocity, as a function of $Z\Gamma^{3/2}$. Here the plasma parameter is introduced as $\Gamma=(e^2/4\pi\varepsilon_0 k_B T)(4\pi n/3)^{1/3}$. The simulation has been performed with three different sets of plasma parameters of $\Gamma=0.11$ (crosses), $\Gamma=0.34$ (triangles), and $\Gamma=1.08$ (circles). The data appear to be almost scaling with $Z\Gamma^{3/2}$. A more careful inspection shows slight deviations from a unique curve. This is due to an explicit temperature dependence besides this scaling from linear theory. This is also confirmed by the RPA result (7). There we plotted three different temperatures of $T=3,5,10$ eV. The lower the temperature the steeper is the increase of the density. These curves are not on one line, indicating the nonlinear character. But the RPA result overestimates the simulation results considerably due to the Z^2 scaling. This is reduced in reality by two-particle collisions which destroy the collective modes.

We see that the Coulomb logarithm approximation (16) can account for the simulation result only up to $Z\Gamma^{3/2}\approx 1$. Then the friction is underestimated due to the $\ln(1+a/Z^2\Gamma^3)$ behavior. The T-matrix result (12) can account for much higher densities $Z\Gamma^{3/2}\approx 3-5$, which is understandable because we account for much higher order correlations due to ladder summation than the Born approximation (16). But for the very strongly coupled case this fails as well.

Connection to transport properties

The stopping power at small velocities yields direct access to the conductivity as a transport property. Therefore we imagine the projectile as a moving current j which causes Joule heat due to friction and a conductivity ρ,

$$\vec{j}\vec{E}=\rho j^2=\rho(neZv)^2=-\langle\dot{E}\rangle. \tag{24}$$

From this consideration we find a direct connection between the dimensionless conductivity $\rho^*=\rho(4\pi\varepsilon_0)^2T^{3/2}/e^2\sqrt{m}$ and a scaled stopping power

$$\lim_{v\to 0}\frac{\lambda v_t}{vT}\frac{dE}{dx}=\frac{Z^2\Gamma^3}{2\pi\sqrt{2}}\rho^*, \tag{25}$$

where $v_t^2=2T/m$ is the thermal velocity and $\lambda=e^2/(12\pi\varepsilon_0 T)$ the Landau length. Consequently, Fig. 11 can be considered also as a scaled plot of the conductivity in a strongly coupled plasma. Therefore the treatment presented here is a generalization of earlier calculations [25], where virial expansions with respect to Γ have been found, to higher coupled plasma $\Gamma\geqslant 1$. This will be further investigated for the strong coupled limit in the next section.

The inspection of Fig. 3 shows that the required limit of small velocities is only possible for mass ratios between projectile and target $m/M\to 0$. Otherwise we would obtain a negative resistivity with a $\approx 1/v^2$ singularity, which is a direct expression of the acoustic Cherenkov effect, see the discussion of the numerical results in Sec. II C.

Now we present approximate results from the T matrix and from the RPA in order to compare to other analytical results. From (12) we obtain a dimensionless conductivity in T-matrix approximation as

$$\rho^*_{tm}=\frac{\varepsilon_0^2\sqrt{2}}{3\sqrt{\pi}Te^4m^3Z^2}\int_0^\infty dpp^5\sigma^t(p)e^{-p^2/2mT}. \tag{26}$$

If we now use the screened Born approximation (20) and carry the function $\Phi(c)=\ln(1+c)-c/(1+c)$ out of the integral at the maximal value of momentum we obtain the result

$$\rho^*_{tm}=\frac{2\sqrt{\pi}}{3}\Phi\left(\frac{2m^2v_t^2}{\hbar^2\kappa^2}\right), \tag{27}$$

with the inverse Debye screening length κ. On the other hand, using now the RPA expression (7), we expand for small velocities and infinite projectile mass and derive

$$\rho^*_{\mathrm{RPA}}=\frac{4\sqrt{2\pi}}{3}\int_0^\infty dk\frac{k^3}{(k^2+\kappa^2)^2}. \tag{28}$$

Using the same cutoff wavelength we have used to derive the Bethe-type formula (9) the result reads

$$\rho^*_{\mathrm{RPA}}=\frac{2\sqrt{2\pi}}{3}\Phi\left(\frac{4m^2v_t^2}{\hbar^2\kappa^2}\right). \tag{29}$$

To compare with the Brooks-Herring result of transport theory [26] one gets in screened Born approximation

$$\rho^*_{\mathrm{BH}}=\frac{\pi\sqrt{2\pi}}{16}\Phi\left(\frac{12m^2v_t^2}{\hbar^2\kappa^2}\right). \tag{30}$$

This result is obtained considering the momentum relaxation as the dominant process. In comparison with the T-matrix

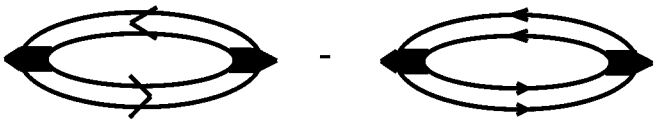

FIG. 12. The next order of the cluster expansion of the polarization function.

result and the RPA result we see the differences in the prefactor as well as the cutoff wavelength. This is due to the energy relaxation which was treated here as the main process in heavy ion stopping.

VI. EXTENSION TO STRONG COUPLING

A. Higher order correlations

The problem of including higher order correlations in the stopping power of strongly coupled plasma is solved by a cluster decomposition of $\Pi(\vec{q},z)$ in the dielectric function (3)

$$\Pi(\vec{q},\omega)=\Pi_1^0(\vec{q},\omega)+\Pi_2^0(\vec{q},\omega)+\cdots, \tag{31}$$

where $\Pi_1^0(\vec{q},z)$ is the one-particle contribution to the polarization function (3) and $\Pi_2^0(\vec{q},z)$ is the two-particle contribution to the polarization function [27], whose graph is given in Fig. 12. The evaluation of this graph can be found in [27–29] with the following expression for the two-particle contribution to the polarization function:

$$\Pi_2^0(\vec{q},\omega)=\sum_{n,n',P}\frac{g(E_{nP}^{ab})-g(E_{n'P+q}^{ab})}{\omega+E_{nP}^{ab}-E_{n',P+q}^{ab}}|M_{nn'}(q)|^2 - \sum_{p_1,p_2}\frac{g(E_{p_1}^{a}+E_{p_2}^{b})-g(E_{p_1+q}^{a}+E_{p_2}^{b})}{\omega+E_{p_1}^{a}-E_{p_1+q}^{b}}. \tag{32}$$

This result for the two-particle polarization function is formally similar to the single-particle polarization function Π^0 in (3). The single-particle (Fermi) distribution $f(E_p)$ has been replaced by the two-particle (Bose) distribution $g(E_{nP}^{ab})=[\exp(E_{nP}^{ab}-\mu_{ab})-1]^{-1}$. The summations over n,n' include bound states as well as scattering states. $M_{nn'}$ is the structure factor of the correlated plasma and μ_{ab} the chemical potential of the bound pair.

The compressibility as an equation of state on the two-particle level can be obtained by [30]

$$K=\frac{1}{n^2}\left(\frac{\partial n}{\partial\mu}\right)_T=\frac{\beta}{n^2}\lim_{q\to 0}\int_{-\infty}^{\infty}d\omega S(q,\omega), \tag{33}$$

where n is the density and μ the chemical potential. The dynamical structure factor $S(q,\omega)$ is linked to the imaginary part of the dielectric function via

$$S(q,\omega)=\frac{1}{\pi V(q)}\frac{1}{e^{\beta\omega}-1}\mathrm{Im}\varepsilon^R(q,\omega). \tag{34}$$

Using (32) the following expression for the compressibility is obtained [29]:

$$K(\beta,\mu)=\frac{1}{n^2}\frac{\beta}{\Omega_0}\Bigg\{\sum_p f_p(1-f_p) +4\sum_{P,\alpha}\int_{-\infty}^{\infty}\frac{dE}{\pi}g\left(E+\frac{P^2}{4m}\right) \times\left[1+g\left(E+\frac{P^2}{4m}\right)\right]D_{\alpha P}(E)\Bigg\}, \tag{35}$$

with D_α given by

$$D_{\alpha P}(E)=c_\alpha\left[\sum_m \pi\delta(E-E_{\alpha mP})+\frac{\partial}{\partial E}\delta_{\alpha P}(E)\right]. \tag{36}$$

It contains the contribution of bound states ($E_{\alpha mP}$) and of scattering states with the scattering phase shift $\delta_{\alpha P}(E)$. Here α denotes the channel of two-particle states, P its total momentum, and m the internal quantum number for the bound states. $g(E)$ is the two-particle (Bose) distribution function including the chemical potentials of both particles, and c_α represents the degeneracy factor of the channel α.

This expression coincides with the compressibility one finds from the Beth-Uhlenbeck formula via (33)

$$n(\beta,\mu)=\frac{1}{\Omega_0}\sum_p f_p+\frac{2}{\Omega_0}\sum_{P,\alpha}\int_{-\infty}^{\infty}\frac{dE}{\pi}g\left(E+\frac{P^2}{4m}\right)D_{\alpha P}(E). \tag{37}$$

Therefore the inclusion of next order cluster expansion in the polarization leads to a consistent equation of state on the level of Beth-Uhlenbeck virial corrections [29].

B. Contribution of ions to the stopping power

Now we evaluate explicitly the influence of the target ions the stopping power. Thus we concentrate on the bound state part of (36) and (37). Following the same steps as presented before we obtain for nondegenerate plasmas

$$\varepsilon=1-\sum_b V_{bb}(\Pi^0+\Pi^0_{\mathrm{bound}}+\Pi^0_{\mathrm{scatt}}). \tag{38}$$

Additionally to the free one-particle polarization function we get a bound and a scattering contribution. The part resulting from the bound state contribution has a structure similar to the free part except for interchanging the mass of the single particle with the mass of the bound state particles and an additional structure factor. From this term follows the well known Saha equation for the relation between free and bound densities in equilibrium,

$$2n_{a+b}=n_a n_b\left(\frac{\lambda_a\lambda_b}{\lambda_{a+b}}\right)^3 \mathrm{e}^{-E_B/T}. \tag{39}$$

Now we give the contribution of the ions with an effective charge Z to the stopping power. For simplicity we choose the approximated RPA result for the polarization function (8) and obtain the stopping power

$$\frac{\dot{E}_a}{n_a}=\frac{Z_a^2e^2}{\varepsilon_0 v(t)}\sum_b\left[\omega_p^2(b)\ln\left(\frac{vk_{\max}}{\omega_p(b)}\right)+\omega_p^2(Zm_b)\ln\left(\frac{vk_{max}}{\omega_p(Zm_b)}\right)\right], \tag{40}$$

where the sum runs over different electron and ion species. Here we signed the mass dependence of the corresponding plasma frequency $\omega(m_a)^2=4\pi e_a^2 n_a/m_a\varepsilon_0$ explicitly. We arrive at the result which is intuitively understandable. The stopping power is given by the sum of electron and ion contributions. One sees that for big mass differences between electrons and ions in a plasma only the electron contribution counts remarkably.

C. Memory effects

An alternative way to consider correlations is due to the concept of memory and retardation on the level of the one-particle distribution. There the evolution of the distribution becomes retarded due to correlations in the system. In [31] an additional collision integral was derived which accounts for the memory in first order gradient approximation

$$\frac{\partial}{\partial T}f_a=\sum_b I_{ab}^B[f]+\frac{\partial}{\partial T}\sum_b I_{ab}^{\rm corr}[f], \tag{41}$$

where I_{ab}^B is the quantum mechanical Boltzmann collision term (11) and $I_{ab}^{\rm corr}$ comes from the retardation expansion,

$$I_{ab}^{\rm corr}=-2\int\frac{dp'_{\mathbf{a}}dp_{\mathbf{b}}dp'_{\mathbf{b}}}{(2\pi\hbar)^6}\delta(p_{\mathbf{a}}+p_{\mathbf{b}}-p'_{\mathbf{a}}-p'_{\mathbf{b}})\times|\langle p_ap_b|\mathcal{T}_{ab}^R|p'_ap'_b\rangle|^2\mathrm{P}'\frac{1}{E_a+E_b-E'_a-E'_b}\times\{f'_af'_b(1\mp f_a)(1\mp f_b)-(1\mp f'_a)(1\mp f'_b)f_af_b\}, \tag{42}$$

where P′ is the derivative of the principal value. The analogous formula holds for the RPA expression. It was shown in [31] that this additional collision integral leads to the same Beth-Uhlenbeck virial correction as given by the cluster decomposition in (37). It accounts for nonideality of the plasma and results in a slower relaxation [16]. We have shown in this way that the memory effect represents higher order correlations which can be alternatively described by cluster decomposition in equilibrium.

D. Stopping power in nonequilibrium

Besides the generalization of the stopping power due to cluster decomposition in the dielectric function (3), which leads to the same equilibrium virial corrections as the memory effects, there are nonequilibrium effects included in the generalized kinetic equation. We will show that this leads to a renormalization of stopping power. From the generalized kinetic equation (41) we find the energy transfer in the form

$$\frac{\partial}{\partial t}\langle E(v)\rangle=\left\langle\frac{p^2}{2m_a}I^B\right\rangle+\frac{\partial}{\partial t}\langle E_{\rm corr}[v(t)]\rangle, \tag{43}$$

where $\langle E_{\rm corr}\rangle=\langle(p^2/2m_a)I_{\rm corr}\rangle$ and the nonideal correction to the stopping power becomes

$$-F[v]=\frac{d}{dx}\langle E\rangle=\frac{1}{v}\left\langle\frac{p^2}{2m_a}I^B\right\rangle+\frac{\dot{v}}{v}\frac{\partial}{\partial v}\langle E_{\rm corr}[v]\rangle. \tag{44}$$

Here we have abbreviated for the correlated term beyond RPA,

$$\langle E_{\rm corr}\rangle=\hbar\frac{2e_a^2}{\pi\varepsilon_0}\frac{1}{v(t)}\int_0^\infty\frac{dk}{k}\int_{-v(t)k+\hbar k^2/2m_a}^{v(t)k+\hbar k^2/2m_a}\times d\omega\,\omega n_B(\omega)\frac{\partial\mathrm{Re}\varepsilon(\hbar k,\omega)/\partial\omega}{|\varepsilon(\hbar k,\omega)|^2}. \tag{45}$$

In contrast to (7) we have here instead of the imaginary part of ε the frequency derivative of the real part. Equation (45) has therefore the same form as (7) but with an additional factor under the integrand which is the inverse of Landau damping $\hbar/\Gamma=\hbar\mathrm{Re}\varepsilon'(\omega_p)/\mathrm{Im}\varepsilon(\omega_p)$, which can be found by linearization of the dispersion relation [32]. In other words, near a collective pole where the Landau damping becomes small the expression (45) can be large and the linearization of memory effects fails.

The differential equation for the projectile velocity reads then in generalization to (22) from (44)

$$\dot{v}=\frac{F[v]_{\rm eff}}{m_a}=\frac{(1/m_av)\langle(p^2/2m_a)I^B\rangle}{1+(1/v)(\partial/\partial v)\langle E_{\rm corr}[v]\rangle/m_a}. \tag{46}$$

We see that the effective stopping power becomes renormalized due to the memory effects, or equivalently nonideality of the plasma. Here we would like to stress that the charge dependence of the stopping power is modified additionally due to the memory effects in (46). A rough estimation can be found choosing the momentum of the Landau damping equal to the thermal one. Then we can write the Landau damping out of the integral. This is in analogy with the Coulomb logarithm approximation, which was performed in (16) from (12), and results here in

$$F_{\rm eff}=\frac{F}{1+(\tau/m_av)(\partial/\partial v)(vF)}, \tag{47}$$

with $\tau=\hbar/\Gamma$ the lifetime of plasmons. This formula is the main result of this section. It shows that the stopping power of the weak coupling theory becomes renormalized by plasmon lifetime effects. Due to the mass of the projectile this renormalization becomes significant only for very dense plasmas.

Using the small momentum expansion the Landau damping can be calculated as [32]

$$\frac{1}{\tau}=\gamma(p)=\hbar\frac{\mathrm{Im}\varepsilon(\omega_p)}{\mathrm{Re}'\varepsilon(\omega_p)}=\hbar V_{bb}\frac{\omega_pn_b\sqrt{\pi}}{2v_tp}(e^{-(p/2m_bv_t)^2}-e^{-(-p/2m_bv_t)^2}). \tag{48}$$

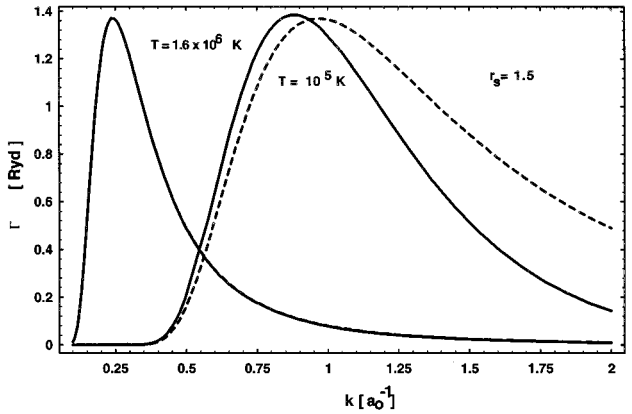

FIG. 13. The Landau damping in dependency on the wave vector for two different temperatures. The density is $6.3\times10^{23}\mathrm{cm}^{-3}$ corresponding to a Bruckner parameter of $r_s=1.5$ in units of the Bohr radius. For lower temperatures the deviation of the classical result (dashed curve) from the quantum mechanical one becomes significant.

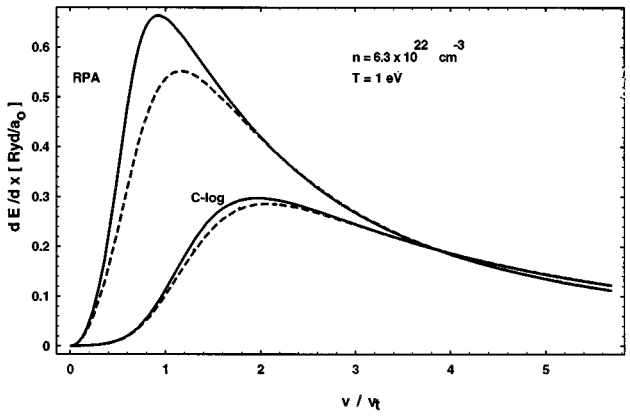

FIG. 14. The enhanced Bethe formula (RPA) from (20) and the Coulomb logarithm formula (C-log) from (16) with (solid) and without (dashed) lifetime effects from retardation.

The classical limit is obvious. In Fig. 13 the Landau damping can be seen for two different temperatures and a density of $6\times10^{23}\ \mathrm{cm}^{-3}$ which corresponds to a Bruckner parameter in units of Bohr radius $r_s=1.5$. The damping is shifted to higher momenta for lower temperatures. Furthermore, the discrepancy between classical and quantum results becomes significant for lower temperatures. With the help of this Landau damping we plotted in Fig. 14 the enhanced Bethe formula (20) together with the Coulomb logarithm approximation (16) with and without lifetime renormalizations. We find an enhancement of the stopping power in the region of the maximum, i.e., around the thermal velocity of the plasma. We suggest that this stopping power formula (47) may serve as a quantitative estimate of the effect of memory or nonideality effects on the stopping power.

VII. SUMMARY

Different approximation schemes have been employed to calculate the stopping power numerically in nonideal dense plasmas. The ladder summation gives more important contributions than the RPA for a dilute plasma at high temperatures. This situation is changed at higher densities and lower temperature. There collective effects, like plasmon emission and absorption, are dominant. This means that the RPA is an appropriate starting point for the calculation of the stopping power. The derivation presented here yields a RPA expression for the stopping power that is valid in any degeneracy of the plasma. This is an extension of former presentations. Different limits are discussed and the range of validity is demonstrated.

A comparison with molecular dynamical simulations was performed. We found a better agreement of the T-matrix approximation for strongly coupled plasmas than the Born-Coulomb logarithm approximation (16). The RPA result overestimates the data considerably. While the Coulomb logarithm approximation and the T matrix follow the scaling law of the linear theory, which is only dependent on $Z\Gamma^{3/2}$, the RPA results show deviations. This can be seen by an explicit temperature dependence. The T matrix describes the behavior well up to plasma parameter of $Z\Gamma^{3/2}=3$. The joint expression between T matrix and RPA shows too high values as well as the RPA itself in comparison with the simulation result. The connection to transport coefficients like friction and conductivity is made. The results presented here are an extension of former small Γ expansions.

Within a model of fast heavy projectiles we solve the equation of motion with the help of the microscopic energy transfer. Using the experimental values for density and temperature in a typical Z-pinch discharge, we are able to reproduce the experimental values of the stopping of $^{238}U^{53+}$ in a hot argon plasma after the pinch.

Further improvement in the calculated stopping power is expected from the inclusion of correlations. We present two alternative schemes to incorporate higher order correlations. One treatment improves the dielectric function by a cluster decomposition. The other approach relies on the inclusion of retardation and memory effects. Both schemes lead to the same quantum virial corrections of Beth-Uhlenbeck type in equilibrium. However, the memory effect results in an additional renormalization of the effective stopping power. This memory effect is controlled by the plasmon lifetime. We found an enhancement of the stopping power in the region of thermal velocity of the plasma for very dense and nonideal plasmas. This lifetime effect results from the retardation. It renormalizes the charge dependency of the stopping power, especially at small velocities.

ACKNOWLEDGEMENTS

The author is grateful for stimulating discussions with G. Zwicknagel, Ch. Stoeckl, R. Walke, and C. Roberts. This work was supported by the BMBF (Germany) under Contract No. 06R0745(0).

APPENDIX A: CALCULATION OF THE COLLISION INTEGRAL

Here we briefly sketch the derivation of Eq. (12) from Eq. (11). First we introduce convenient coordinates via

$$p' = \frac{m_a}{M} p_b' - \frac{m_b}{M} p_a',$$

$$K' = p_a' + p_b' \tag{A1}$$

such that the momentum distribution function can be written as $\delta(\Delta p) = \delta(K' - K)$ and the energy conservation becomes $\delta(\Delta E) = 2\mu\delta(p^2 - p'^2)$, where μ is the reduced and M the total mass of colliding particles. Secondly the quantum differential cross section can be found from the T matrix by

$$\frac{2\pi\mu}{\hbar}\int_0^\infty \frac{p'^2 dp'}{(2\pi\hbar)^3}\delta(p'^2 - p^2)\left|\left\langle p\left|T\left(K, \frac{K^2}{2M} + \frac{p^2}{2\mu}\right)\right|p'\right\rangle\right|^2 = \frac{p}{2\mu}\frac{d\sigma}{d\Omega}\left(\Omega, \frac{p^2}{2\mu}\right). \tag{A2}$$

Here we neglected the center of mass momentum dependence of the cross section, which would enter only for in-medium cross sections. The collision integral (11) becomes then

$$I_{\text{Boltz}}(p) = \frac{1}{\mu}\int \frac{dp_b}{(2\pi\hbar)^3}\int d\Omega' p \frac{d\sigma}{d\Omega}\left(\Omega', \frac{p^2}{2\mu}\right) \times [f_{a'} f_{b'} \overline{f_a f_b} - f_a f_b \overline{f_{a'} f_{b'}}], \tag{A3}$$

with $K = p_a + p_b$ and $p = (m_2/M)p_a - (m_1/M)p_b$. Multiplying this collision integral with $p^2/2m_a$ and integrating over the momentum p_a we derive the energy transfer. Using the Boltzmann distribution functions for the target f_b and the delta distribution $f_a(p) = (2\pi\hbar)^3 n_a \delta(p - u(t))$ for the projectile we obtain

$$\frac{\dot{E}_a}{n_a} = \frac{n_b \lambda_b^3}{\mu}\int \frac{dp dK}{(2\pi\hbar)^6}\frac{p^2 K}{M} e^{-[p-(m_b/M)K]^2/2m_b T} \times \delta\left(u - p - \frac{m_a}{M}K\right)\int d\Omega'(\cos\alpha - \cos\alpha')\frac{d\sigma}{d\Omega}(\alpha', p)$$
$$= \frac{n_b \lambda_b^3}{\mu}\int \frac{dp dK}{(2\pi\hbar)^6} p \frac{pK}{M} e^{-[p-(m_b/M)K]^2/2m_b T} \times \delta\left(u - p - \frac{m_a}{M}K\right)\sigma^t(p), \tag{A4}$$

where angular relations are used and the transport cross section (13) was introduced. After straightforward algebra and trivial integrals we end up with Eq. (12).

APPENDIX B: SUM RULES

The sum rules used can be found easily in the following way:

$$\int_{-\infty}^{+\infty} d\omega \omega n_B(\omega) \text{Im}\varepsilon^{-1}(\omega) = \int_0^{+\infty} d\omega \omega n_B(\omega) \text{Im}\varepsilon^{-1}(\omega) + \int_0^{+\infty} d\omega \omega n_B(-\omega) \text{Im}\varepsilon^{-1}(\omega) = -\int_0^{+\infty} d\omega \omega \text{Im}\varepsilon^{-1}(\omega) = \frac{\pi}{2}\omega_p^2. \tag{B1}$$

Here we used the fact that $\text{Im}\varepsilon(\omega)$ is an odd function and $n_B(-\omega) = -1 - n_B(\omega)$. The sum rule for the last equality can be found in any textbook. A related sum rule reads analogously

$$\int_{-\infty}^{+\infty} d\omega \omega n_B(\omega) \text{Im}\varepsilon(\omega) = -\frac{\pi}{2}\omega_p^2. \tag{B2}$$

[1] N. A. Tahir, D. H. H. Hoffmann, J. A. Maruhn, and C. Deutsch, Plasma Phys. Control. Fusion **37**, 447 (1995).
[2] J. Jacoby *et al.*, Phys. Rev. Lett. **74**, 1550 (1995).
[3] T. Peter and J. Meyer-ter-Vehn, Phys. Rev. A **43**, 1998 (1991).
[4] D. H. H. Hoffmann *et al.*, Phys. Rev. A **42**, 2313 (1990).
[5] I. Hofmann, in *Proceedings of the Workshop on Beam Cooling and Related Topics* (CERN, Switzerland, 1994), p. 330.
[6] G. Zwicknagel, C. Toepffer, and P. G. Reinhard, Laser Part. Beams **13**, 311 (1995).
[7] J. Bosser, in *Proceedings of the Workshop on Beam Cooling and Related Topics* Ref. [5].
[8] C. Deutsch and N. A. Tahir, Phys. Fluids B **4**, 3735 (1992).
[9] C. Deutsch, Laser Part. Beams **10**, 217 (1992).
[10] A. Bret and C. Deutsch, Phys. Rev. E **47**, 1276 (1993).
[11] C. Deutsch, Phys. Rev. E **51**, 619 (1995).
[12] D. Klakow, C. Toepffer, and P. G. Reinhard, Phys. Lett. A **192**, 55 (1994).
[13] W. D. Kraeft and B. Strege, Physica A **149**, 313 (1988).
[14] H. H. Brouwer *et al.*, Contrib. Plasma Phys. **30**, 263 (1990).
[15] H. H. Brouwer *et al.*, Contrib. Plasma Phys. **30**, 369 (1990).
[16] K. Morawetz, R. Walke, and G. Roepke, Phys. Lett. A **190**, 96 (1994).
[17] K. Morawetz, Phys. Rev. E **50**, 4625 (1994).
[18] S. Ichimaru, *Basic Principles in Plasma Physics* (Benjamin, Reading, MA, 1973).
[19] G. Röpke and R. Redmer, Phys. Rev. A **39**, 907 (1989).
[20] G. Zwicknagel, Ph.D. thesis, University Erlangen, 1994 (unpublished).
[21] H. A. Gould and E. H. DeWitt, Phys. Rev. **155**, 68 (1967).
[22] R. H. Williams and E. H. DeWitt, Phys. Fluids **12**, 2326 (1969).
[23] G. Zwicknagel, C. Toepffer, and P. G. Reinhard, Nuovo Cimento A **106**, 1857 (1993).
[24] H. Wetzler *et al.*, in *Proceedings of the International Conference on Physics of Strongly Coupled Plasmas*, edited by M. S. W. D. Kraeft (World Scientific Publishing, Singapore, 1996), p. 357.

[25] G. Röpke, Phys. Rev. A **38**, 3001 (1988).
[26] H. Brooks, Phys. Rev. **83**, 879 (1951).
[27] G. Röpke and R. Der, Phys. Status Solidi B **92**, 501 (1979).
[28] G. Röpke, C. V. Meister, K. Kollmorgen, and W. D. Kraeft, Ann. Phys. (Leipzig) **7**, 377 (1979).
[29] G. Röpke, K. Morawetz, and T. Alm, Phys. Lett. B **313**, 1 (1993).
[30] N. D. Mermin, Ann. Phys. (N.Y.) **18**, 421 (1962).
[31] K. Morawetz and G. Röpke, Phys. Rev. E **51**, 4246 (1995).
[32] W. D. Kraeft, D. Kremp, W. Ebeling, and G. Röpke, *Quantum Statistics of Charged Particle Systems* (Akademie Verlag, Berlin, 1986).
[33] H. Wetzler *et al.*., in *High Energy Density in Matter*, edited by D. H. H. Hoffmann, I. Hofmann, and J. Meyer-ter-Vehn, GSI-Jahresbericht 1994 (GSI, Darmstadt, 1995), p. 11.